Microstructure effects on static and dynamic moduli for two sandstones

Yang Wang*, De-hua Han, and Jiali Ren, Rock Physics Lab, University of Houston; Yonghao Zhang, China Petroleum Logging Co., Ltd; Luanxiao Zhao, Tongji University

Summary

In this experimental investigation, we adopt a stepwise way to process the stress-strain curves to reflect the nonlinear properties of porous sandstones. It is always sure the static moduli are characteristically lower than dynamic moduli. However, the static moduli under different stress conditions display different change trends. From microstructural aspects, we believe grain contact area enlarging is the primary reason for the increasing static bulk moduli under hydrostatic load. And the static frictions along grain boundaries prevent any movements and make the rocks behave elastically. Under triaxial load, the gradual conversion from static to dynamic frictions lead to dramatic drops of static Young's moduli. Moreover, at the initial triaxial unload, the shear stress needed to reverse the frictional sliding would decrease to zero firstly and then increase in an opposite manner, which result in a much higher static modulus compared with that at the end of triaxial load.

Introduction

In reservoir and drilling engineering, static properties such as bulk modulus and Young's modulus are needed in hydraulic fracturing designs. Directly obtaining such data is highly limited by the core availability and financial constraints. Usually, dynamic moduli derived from laboratory or sonic log measurements are used to predict the corresponding static properties. But different measuring mechanisms decide that straightforward conversion between static and dynamic moduli is unreasonable. In order to properly relate acoustic velocity measurements from full-waveform sonic logs to mechanical properties, possible reasons for their discrepancies are supposed to be considered and discussed.

From the first order, the corresponding static and dynamic moduli are equal for nonporous materials like nickel, copper, and aluminum (Bristow, 1960). It is still true for stiff minerals like quartz and calcite based on the research from Darling et al. in 2004. But for porous sandstones, except for those stiff minerals, there are soft minerals, soft pores and grain boundaries. The heterogeneity of porous medium brings great challenges in the evaluation of static and dynamic moduli (Holt et al., 2013).

In rock mechanics literatures, it is widely accepted to measure only the loading portion of the stress-strain curve to obtain static modulus. But for true rocks, the strains respond nonlinearly to the applied stress. It is difficult to find a real linear portion for deriving a certain static modulus. Additionally, the loading and unloading stress-strain curves often show different characteristics (Hilbert et al., 1994; Fiona and Cook, 1995).

In this study, we perform hydrostatic load and triaxial load-unload tests on two porous sandstones. Being different from the traditional static modulus derivation method, we process the stress-strain curves stepwisely. Through analysis, we strive to emphasize the effects of microstructures like grain contact, static and dynamic frictions on the static and dynamic properties.

Sample descriptions and experimental set-up

Sandstone samples undergone measurements come from two geological outcrops: Berea and Idaho Gray. Porosity and grain density are: 23.22% and 2.62 g/cm^3 for Berea, 33.3% and 2.57 g/cm^3 for Idaho Gray. Big porosity differences are convenient for comparative analysis of the experimental results. Thin section images taken under cross-polarized light are shown in Figure 1. The microstructures are mainly constructed out of medium grains with argillaceous cement. Detrital grains are mainly composed of angular or sub-rounded quartz for Berea sandstone, and angular quartz and feldspar for Idaho Gray sandstone. Intergranular pores are more developed in Berea than Idaho Gray.
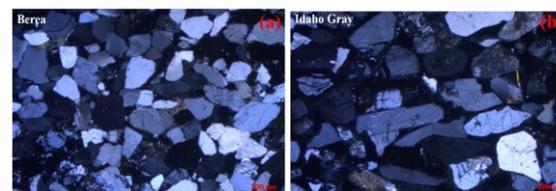

Figure 1: Thin section images for two samples, (a) Berea sandstone is composed of angular quartz mainly with point contacts, (b) Idaho Gray sandstone is composed of angular quartz and feldspar with surface contacts.

Experiments are conducted with the Auto 1500 triaxial apparatus in China Petroleum Logging Company. Cylindrical samples with 1.5-inch diameter are measured under hydrostatic and triaxial stress conditions with no pore pressure. The axial strain is measured with linear variable differential transformers (LVDT), while radial strain is measured with one pair of strain gauges on side. The through-transmission technique with 1 MHz central frequency for P- and S-wave is adopted for ultrasonic velocity measurements. Only axial P- and S- wave

velocities are measured every 5 MPa interval. Figure 2 shows the experimental procedures for two sandstones. Firstly, the confining pressure is applied to 20 MPa (hydrostatic stage) with a step of 0.2 MPa/s. Then, differential stress is applied in the axial direction to ~25 MPa for Berea sandstone and ~15 MPa for Idaho Gray sandstone (triaxial stage) with a step of 0.02 MPa/s. The differential stress is kept constant for around 1 hour between loading and unloading. During triaxial tests, the confining pressure is kept at 20 MPa to ensure closure of most microcracks and reduce the effect of open microcracks in our analysis. The reason for applying different differential stresses to two samples is to avoid the damage of the soft Idaho Gray sandstone.
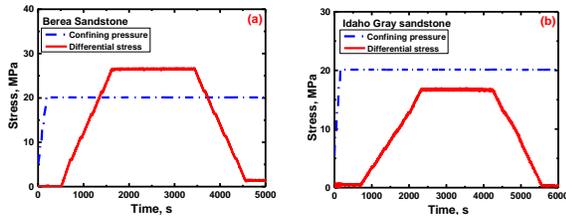

Figure 2: Experimental procedures for (a) Berea sandstone and (b) Idaho Gray sandstone.

Figure 3 displays details for the stress-strain relations for both samples. During hydrostatic stage, the axial strain (black curves) almost exactly overlaps with the radial strain (red curves) for Idaho Gray sandstone (Figure 3(b)), which indicate it is isotropic. Meanwhile, the axial strain changes a little more than the radial for Berea sandstone (Figure 3(a)). Under triaxial stage, axial strain changes along compression direction while radial strain changes along expansion direction. The 1 hour-stabilization brings about more volumetric strain creeping for Idaho Gray sandstone because of the relatively higher porosity. After unloading back to the original point of triaxial tests, Idaho Gray sandstone displays more unrecoverable strains.
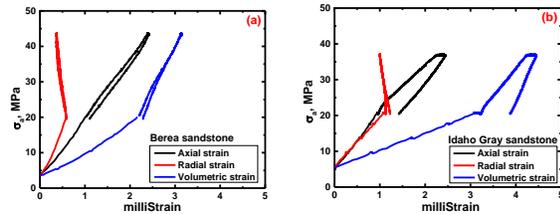

Figure 3: Stress-strain relations in the whole process for (a) Berea sandstone and (b) Idaho Gray sandstone.

Hydrostatic stage

The black solid curves in Figure 4 show mean stress-volumetric strain relationships for two samples. The tangential slopes of these two curves are the static bulk

moduli, which could be derived from Equation 1. The dynamic bulk modulus is able to be calculated from Equation 2.

$$K_{sta} = \frac{\Delta \sigma_{mean}}{\Delta \varepsilon_{vol}}$$

$$\varepsilon_{vol} = \varepsilon_a + 2\varepsilon_r \qquad (1)$$

$$\sigma_{mean} = \frac{\sigma_a + 2\sigma_r}{3}$$

$$K_{dyn} = \rho(V_p^2 - \frac{4V_s^2}{3}) \qquad (2)$$

Where, K_{sta} and K_{dyn} are the static and dynamic bulk modulus, GPa; σ_a and σ_r are the axial and radial stress, MPa; ε_a and ε_r are the axial and radial strain, 10^{-3}; σ_{mean} is the mean stress, MPa; ε_{vol} is the volumetric strain, 10^{-3}; ρ is the bulk density, g/cm^3; V_p and V_s are the ultrasonic P- and S-wave velocities, km/s.
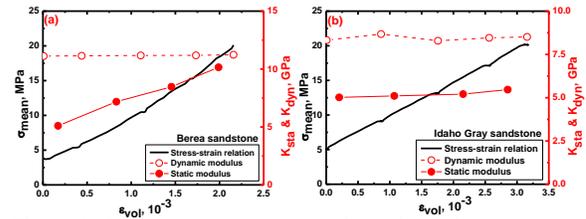

Figure 4: The mean stress (σ_{mean})-volumetric strain (ε_{vol}) curves under hydrostatic load, and static (K_{sta}) and dynamic (K_{dyn}) modulus vs. volumetric strain for (a) Berea sandstone and (b) Idaho Gray sandstone.

The small creeps in the black curves are caused by stopping for velocity measurements. Between the adjacent two creeps, strain responses linearly to stress in all cases. Considering theses, we adopt a stepwise method to derive the static bulk moduli, as shown with red solid circles with solid lines in Figure 4. The red open circles with dashed lines are for dynamic bulk moduli. For Berea sandstone with many point contacts (in Figure 1(a)), compared with the slight increase of the dynamic moduli with the increasing hydrostatic stress, the static moduli display dramatic increments. From Hertz-Mindlin theory, the areas initially without contacts would contact together, leading to the increase of coordinate number; the areas initially with point contacts would get enlarged. All these will result in the stiffer and stiffer behavior of Berea sandstone. Therefore, both the dynamic and static bulk moduli would present increasing trends. But a pulse of elastic wave may be expected to choose stiff frames to propagate in priority and bypass microcracks and soft pores (Simmons and Brace, 1965). The enlarged grain contact area and soft pore compactions would bring less effects on the dynamic velocities than the static properties. With the increasing compaction, the static moduli gradually approach the dynamic moduli but never exceed, and the dynamic modulus serves as the upper bound of static modulus.

Static and dynamic moduli

However, for Idaho Gray sandstone, in Figure 1(b), the grain contacts have reached relatively stable states mainly with surface contacts. Therefore, the increasing hydrostatic stress will bring much less effect on both static and dynamic moduli, as shown in Figure 4(b). This phenomenon is common in some soft sandstones with large porosity (Han, 1986).

Triaxial stage

During triaxial stage, the confining pressure is kept at 20 MPa for both samples, which makes sure the microcrack closure and soft pore compaction have been completed. The axial stress is applied up to ~45 MPa for Berea sandstone and ~35 MPa for Idaho Gray sandstone, which are ~50% of their failure strengths. We treat the static modulus in these measurements as static Young's modulus, although the measurements are not under uniaxial stress conditions. The static Young's modulus is able to obtain from the slope of stress-strain curve by using Equation 3. Meanwhile, the dynamic Young's modulus is able to be calculated with Equation 4.

$$E_{sta} = \frac{\Delta \sigma_a}{\Delta \varepsilon_a} \qquad (3)$$

$$E_{dyn} = \rho V_s^2 \left(\frac{3V_p^2 - 4V_s^2}{V_p^2 - V_s^2} \right) \qquad (4)$$

Where, E_{sta}, E_{dyn} are the static and dynamic Young's moduli respectively, GPa; σ_a is the axial stress, MPa; ε_a is the axial strain, 10^{-3}; ρ is the bulk density, g/cm^3; V_p and V_s are the ultrasonic P- and S-wave velocities, km/s.

Figure 3 also displays the axial stress-strain relationships in the process of "load-stabilize-unload". From the whole, the sample with larger porosity is more affected by the 1-hour creeping, leading to much larger unrecoverable strains when differential stress falls back to 0. Moreover, the unloading curves tend to be more linear than the loading curves. In order to obtain more details from these nonlinear behaviors, a stepwise way to process the curves is adopted.

Figure 5 shows the stepwise static moduli for both loading (red solid circles with solid lines) and unloading (red open circles with dashed lines), together with the dynamic moduli (black circles with lines). Several phenomena could be described as follows:

- The odd static modulus for Idaho Gray sandstone at the initial loading may be caused by the interlocking of the asperities.
- The dynamic moduli act as the upper bound of static moduli. And with applying differential stress, static moduli behave dramatically decreasing trends.

- At the very beginning of unloading, static moduli firstly jump to much higher values, and then decrease.
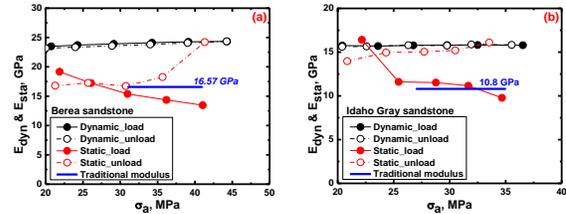

Figure 5: Static (E_{sta}) and dynamic (E_{dyn}) Young's moduli vs. axial stress (σ_a) during triaxial load and unload for (a) Berea sandstone and (b) Idaho Gray sandstone.

Traditionally, the tendency is to measure only the loading portion to obtain the tangential modulus (blue lines in Figure 5). But our measuring data demonstrates that the actually nonlinear stress-strain curves bring about great challenges in which portion is supposed to be used for calculation. Additionally, the unloading static moduli, which are more close to elasticity, are totally different from the loading counterparts. Primarily, the mechanisms leading to these different trends should be made clear.
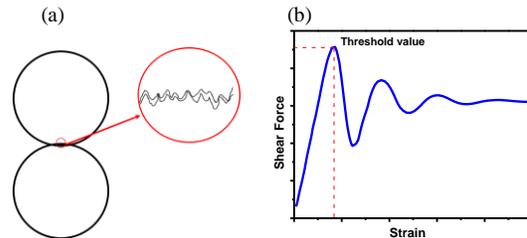

Figure 6: (a) grain contact model with randomly distributed asperities on the surface (modified after Brilliantov et al., 1996), (b) a model for converting from static to dynamic frictions (modified after Farkas et al., 2005).

After hydrostatic load, we assume the microcrack closure and soft pore compaction have already been finished. There is a high possibility that the enlarged grain contact surfaces have randomly distributed asperities, as shown with a simple model in Figure 6(a). The shear stress, which is proportional to the stress normal to the grain contact area, is not large enough to break the interlocking structures and make relative movements. With applying differential stress, the shear stress attempts to overcome the static frictions. Figure 6(b) shows a simple model for conversion from static to dynamic friction, modified after Frarkas et al. 2005. The friction force here is proportional to the external driving force. The first peak force is the threshold value for initiating motion. Once the movement occurs, the friction force needed for maintaining movements decays to a much smaller value with damped oscillations. Obviously, converting from static to dynamic frictions would decrease

the modulus. And the modulus at the initial motion may reverse to a negative value.

With these foundations, we analyze the data within 1 MPa stress range, as an example for Idaho Gray sandstone shown in Figure 7. The detailed stress-strain curve shows a step-like behavior. Initially, axial strain has no response to increasing axial stress. After reaching a threshold value, the axial stress suddenly drops together with increasing axial strain. This is similar to the process of conversion from static to dynamic friction in Figure 6(b). In the heterogeneous sandstones, some grain contact surfaces with low threshold amplitude will slide firstly, while others with much higher threshold values will gradually begin to move with the increasing applied differential stress.
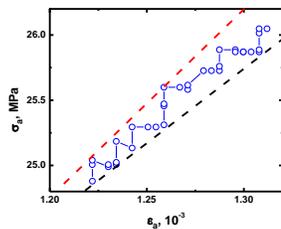

Figure 7: Detailed information within 1 MPa axial stress (σ_a) for Idaho Gray sandstone. Open circles with solid lines show step-like stress-strain relation; dashed lines display the bounds for the points at the initial dynamic frictions and after dynamic frictions.

One hour-creeping makes sure more grain rearrangements and allows the rock to behave more elastically (Hagin and Zoback, 2004). More importantly, at the initial unload, the shear stress will firstly decrease to zero and then increase in an opposite manner (Walsh, 1965; Fiona and Cook, 1995). That means the shear stress on the grain boundaries would change by twice the threshold value to realize reversed sliding. Therefore, when the load is reversed, the opposite frictional sliding will not occur immediately. And the initial unload static modulus is closer to the dynamic counterpart with a much high value.

Discussions

Strains always response nonlinearly to stress in porous sandstones. After stepwisely processing the nonlinear stress-strain curves, static moduli display different change trends under hydrostatic and triaxial stages, while dynamic moduli always increase with loading and decrease with unloading. The relatively larger variations of static moduli compared with dynamic moduli can be attributed to that a pulse of elastic wave in priority chooses stiff frames to propagate and bypasses microcracks and soft pores, while small strain changes would bring large changes in static modulus.

Under hydrostatic loading, the top stress is ~20 MPa, which is far below the threshold stress for pressure solution and grain crushing (Zhang et al., 1990). In addition, for sandstones except for unconsolidated sands, the relative porosity changes are hard to exceed 2% (Han, 1986). So, the soft pore compaction and porosity decrease are not the first-order reasons for the dramatic static modulus variations. We believe the elastic compaction, which satisfies Hertz-Mindlin theory, is responsible for the increasing trends of static bulk modulus. The enlarged grain contact area makes the rock stiffer and stiffer. And the increasing static modulus infinitely approaches but never exceeds the dynamic modulus, which serves as the upper bound.

Under triaxial loading, the shear stress, which is proportional to the applied differential stress, will strive to convert the static frictions on the grain boundaries to dynamic frictions. Once the motion occurs, the shear stress and differential stress will drop together with increasing strains. With the increase of differential stress, more and more conversions will occur. This is the primary reason for the decreasing trend of static Young's modulus. However, when the load is reversed, the shear stress will decrease to zero firstly and then increase in an opposite sense to realize the reversed sliding. Therefore, the static Young's modulus at the initial unload is much closer to elasticity with a high value.

Conclusions

Time-dependent dynamic modulus serves as the upper bound of the time-independent static modulus. After stepwise analysis of the stress-strain curves, static moduli will approach to or departure from the upper bound due to different microstructural mechanisms. The elastic compaction with enlarging grain contact area is the dominant reason for the increasing static bulk modulus under hydrostatic loading. Also, under this stage the static frictions on the grain boundaries allow the rocks to behave elastically. Once the differential stress is applied, the conversion from static to dynamic frictions will gradually occur, which is the primary reason for the decreasing static Young's modulus under triaxial loading. At the initial unload, the reverse of fictional sliding would not immediately occur, which results in a higher static Young's modulus.

Acknowledgements